Structural and Photophysical Properties of Peptide Micro/Nanotubes Functionalized with Hypericin

ARTICLE *in* THE JOURNAL OF PHYSICAL CHEMISTRY B · MARCH 2013

Impact Factor: 3.3 · DOI: 10.1021/jp3113655 · Source: PubMed

THE JOURNAL OF PHYSICAL CHEMISTRY B

Article

pubs.acs.org/JPCB

Structural and Photophysical Properties of Peptide Micro/Nanotubes Functionalized with Hypericin

Márcia I. Souza,[†] Ygor M. Jaques,[†] Gislaine P. de Andrade,[†] Anderson O. Ribeiro,[†] Emerson R. da Silva,[†] Eudes E. Fileti,[‡] Érick de Souza Ávilla,[§] Maurício V. B. Pinheiro,[§] Klaus Krambrock,[§] and Wendel A. Alves*[,†]

[†]Centro de Ciências Naturais e Humanas, Universidade Federal do ABC, 09210-170, Santo André, SP, Brazil

[‡]Instituto de Ciência e Tecnologia, Universidade Federal de São Paulo, 12231-280, São José dos Campos, SP, Brazil

[§]Departamento de Física, ICEx, Universidade Federal de Minas Gerais, 31270-901, Belo Horizonte, MG, Brazil

Supporting Information

ABSTRACT: Hypericin is a photosensitizer with promising applications in photodynamic therapy (PDT) for cancer and infectious diseases treatments. Herein, we present a basic research study of L-diphenylalanine micro/nanotubes (FF-NTs) functionalized with hypericin. The system has special properties according to the hypericin concentration, with direct consequences on both morphological and photophysical behaviors. A clear dependence between the size of the tubes and the concentration of hypericin is revealed. The generation of reactive oxygen species (ROS) is found to be improved by ∼57% in the presence of FF-NTs, as indirectly measured from the absorbance profile of 1,3-diphenylisobenzofuran (DPBF). In addition, when hypericin appears conjugated with FF-NTs, the characteristic fluorescence lifetime is significantly boosted, demonstrating the role of FF-NTs to enhance the photophysical properties and stabilizing the fluorophore in excited states. Electron paramagnetic resonance allows the proposition of a mechanism for the generation of ROS. Molecular dynamics simulations bring new insights into the interaction between hypericin and peptide assemblies, suggesting the spatial organization of the fluorophore onto the surface of the supramolecular structures as a key element to improve the photophysical properties reported here.

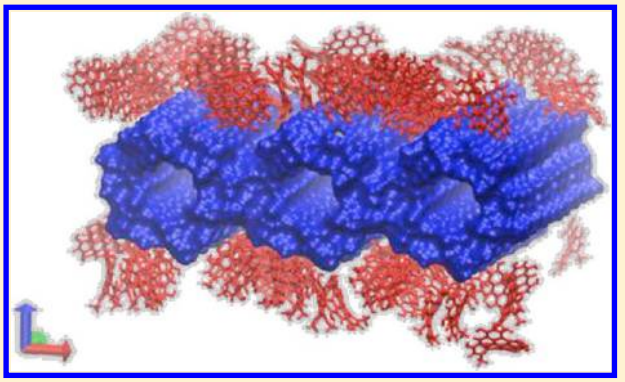

INTRODUCTION

Molecular self-assembly is a design technique that involves noncovalent interactions. Peptides with aromatic residues — for example, L-diphenylalanine (FF) — can self-assemble into 1D tubular structures,[1] in which $\pi-\pi$ interactions or hydrogen bonding play a vital role in stabilizing the structure and the fibers.[2,3] The self-assembly of peptide-based building blocks into ordered nanomaterials is a common phenomenon in many natural systems. A traditional example involving L-diphenylalanine is the formation of amyloid fibrils, which are associated with a considerable number of human diseases, including Alzheimer's disease and type-II diabetes.[4,5]

Peptide nanotubes are an attractive group of supramolecular assemblies because of their molecule recognition abilities and potential for a wide range of surface chemical modifications.[6−12] The functionalization of these nanomaterials with transition-metal nanoparticles,[13] polymers,[14] and photoluminescent compounds,[15] among others, has increased the range of applications for FF-NTs. These factors play a key role in several biological applications, including photosensitizer carrier systems, the focus of this study. Recently, a hydrogen peroxide biosensor was developed by combining the well-known properties of microperoxidase-11 (MP11) as an oxidation catalyst with the interesting characteristics of L-diphenylalanine peptide nanotubes as a supporting matrix to provide a good bioelectrochemical interface.[16] The FF-NTs provide a favorable microenvironment for MP11 to perform direct electron transfer to the electrode surface.

The conjugation of pyrenyl-1-carboxylic acid with L-diphenylalanine nanotubes was also recently investigated, and the effects of pH and fluorophore concentration were evaluated. The results showed that these parameters have a strong influence on the final morphology and photophysical response of the assembled nanostructures.[17] Therein, these findings appear related to the protonation state of the carboxyl groups either at the pyrenyl chromophore or at the FF molecules, revealing that the fibril structure is driven by a delicate balance between electrostatic and hydrophobic forces.

In this work, we carry out a basic research study and demonstrate the functionalization of peptide micro/nanotubes

Received: July 30, 2012
Revised: February 8, 2013

   dx.doi.org/10.1021/jp3113655 | J. Phys. Chem. B XXXX, XXX, XXX−XXX

with hypericin and the improvement of the photophysical properties of the fluorophore emerging from this conjugation. Apart from a basic research interest, we believe that this system could bring insights into hybrid fluorophore/peptide compounds and contribute to disclose the potential of peptide assemblies in photodynamic therapy (PDT).

Hypericin (Hyp) is a natural photosensitizing pigment that occurs in plants of the genus Hypericum (the most common of which is Saint John's Wort).[18,19] This ethanolic extract has long been used in traditional medicine as a coadjuvant in the treatment of depression and wound healing. More recently, it has been extensively studied for use in PDT because they have an appreciable quantum yield for production of reactive oxygen species (ROS) when irradiated with visible light (550−600 nm).[20−22]

PDT requires a photosensitizer, an appropriate light source, and molecular oxygen. ROS are formed upon excitation of the photosensitizer. When these species are oxygen radicals formed through a charge transfer from the photosensitizer, the process is called type I. When oxygen singlet ($^1O_2$) is produced after light excitation by a resonant energy transfer from the photosensitizer, the process is of type II. Years ago, it was demonstrated that $^1O_2$ is responsible for most of the photodynamic activity found in hypericin. The formation of superoxides or hydroxyl radicals was estimated to be very low because the sum of quantum yields due to both oxygen singlet production and fluorescence of hypericin was found to be close to unity.[23] However, oxygen radicals play an important role in the therapeutic effect being often produced in a secondary step. Therefore, the elucidation of the mechanisms involved in the photoactivation of the sensitizer is a major concern.

Hypericin compounds suffer from cytotoxicity and aggregation in aqueous environment. This drawback may be reduced by the use of macromolecules as a carrier system, thus becoming highly fluorescent monomers.[24] Whereas most of PDT therapies known are used against cancer, a compound containing hypericin could be employed in the treatment of infectious diseases caused by microorganisms.[25] In some cases, such as cutaneous leishamniasis, topical PDT can also be used,[26−29] and for this type of treatment, the low aqueous solubility of certain photosensitizers − including hypericin − is not detrimental. Futhermore, fluorescence measurements have also shown that Hyp does significantly interact with peptides in β-sheet conformation and inhibit fibrillogenesis through interactions with β-sheet portions of β-amyloid peptide oligomers.[30] Thus, proteins and their peptide fragments can be used as potential sources for development smart function materials.

Motivated to use the L-diphenylalanine aromatic module as a minimal amyloidogenic fragment and as a model system for other functionalized peptide nanostructures, we investigate the effects of the hypericin concentration on the nanotube structure and the new photophysical properties by using microscopy and spectroscopy techniques. Furthermore, computational simulations reveal details of the functionalization of the peptide nanotube with hypericin, thereby providing a full characterization of the structural and dynamic properties of this new material.

EXPERIMENTAL SECTION

Materials. Dipeptide L-diphenylalanine, 1,3-diphenylisobenzofuran (DPBF), 1,1,1,3,3,3 hexafluor-2-propanol (HFP), α-phenyl-*N*-*tert*-butyl nitrone (PBN) spin-trap, methyl alcohol, dimethyl sulfoxide (DMSO), chloroform, and isopropylmyristate (IPM) were purchased from Sigma-Aldrich (USA) and Synth (Brazil). Ultrapure water ($R > 18$ mol L^{-1} Ω cm^{-1}) was used to self-assemble the dipeptides via hydrophobic effect. The hypericin was synthesized using previously reported methods.[31,32]

Nanotube Preparation. The functionalized peptide nanotubes were prepared by diluting 3 mg of L-diphenylalanine in HFP (30 μL) and then adding an aliquot of hypericin in methanol (1.25×10^{-3} mol L^{-1}). The concentration of hypericin in the final solution for each sample is indicated in Table 1. The solutions were vortexed for several minutes. Next,

Table 1. FF-NT/Hyp Samples with Different Hyp Concentrations

sample	concentration (μmol L^{-1})	sample	concentration (μmol L^{-1})
1	0.7	7	4.2
2	0.9	8	4.6
3	1.8	9	5.5
4	2.1	10	6.0
5	2.9	11	8.0
6	3.7	12	10

150 μL of ultrapure water was added and the functionalized FF-NTs were centrifuged at 12 000 rpm at room temperature for 20 min. The supernatant was then removed. We have assumed that all Hyp was adsorbed onto the surface of NTs, and thus the amount of fluorophore conjugated with the peptide structures is that one used in the synthesis procedure. In addition, we have also considered that all fractions of peptides in solution were converted on NTs.

Structural, Morphological, and Physical Characterization. X-ray diffraction (XRD) patterns of powdered samples were recorded at room temperature on a D8 Focus Discover diffractometer (Bragg−Brentano configuration). The beam was provided by a Cu-target source, $\lambda = 0.154$ nm, operating at 40 kV/30 mA. The 2θ range was scanned between 5 and 30°. Scanning electron microscopy (SEM) images were obtained using a JEOL FEG-SEM JSM 6330F or a JEOL LV-SEM microscope at the LME/LNLS (Laboratory of Electron Microscopy of the Brazilian Synchrotron Light Laboratory, Campinas, Brazil). Fluorescence microscopy images were obtained using an Axio/ZEISS (λ_{exc} = 550 nm) inverted fluorescence microscope. Atomic force microscopy (AFM) imaging was carried out using a Digital Instruments Nanoscope III (further details are given in the Supporting Information (SI)) at the LNNano (Brazilian Nanotechnology National Laboratory, Campinas). The oxidation of the DPBF (45 μmol L^{-1}) was characterized by UV/vis absorption recorded on a VARIAN 50 scan spectrophotometer. The light source was an illumination diffusion table composed of yellow LEDs (predominantly 590 nm). The output power was kept constant at 10 mW cm^{-2}, and the fluence of 6 J cm^{-2} was obtained by 10 min of illumination. The absorbance was simultaneously monitored in the range 350−700 nm by using the spectrophotometer in the kinetic mode. Fluorescence lifetimes were measured using a time-correlated single photon counting (TCSPC) FL-900 spectrophotometer from Edinburgh Analytical Instruments, which uses a pulsed hydrogen arc lamp with a repetition rate of 40 kHz. The fluorescence maximum of Hyp (λ_{em} = 594 nm) was used as the emission wavelength for the TCSPC measurements. Solid samples were aligned at 45° to

dx.doi.org/10.1021/jp3113655 | J. Phys. Chem. B XXXX, XXX, XXX−XXX

the incident radiation, and the emission was collected at a right angle from the front face of the sample. The samples were sealed under vacuum to avoid oxygen suppression of the fluorescence. The instrument response was determined using Ludox as a scatterer. At least 10^4 counts were collected in the peak channel. Deconvolution of the lamp pulse was performed using a nonlinear least-squares routine in the software supplied by Edinburg Analytical Instruments. The χ^2 value closest to unit indicated the good quality of the fits.

Electron paramagnetic resonance (EPR) measurements were performed using a custom-built X-band spectrometer (9.38 GHz) and a commercial cylindrical cavity (Bruker). The Klystron microwave source (Varian) provided ~100 mW, which could be attenuated down to 60 dB. The magnetic field was produced using an electromagnet (Varian) and an automated current source (Heinzinger). Standard lock-in techniques (EG&G) and a 100 kHz field modulation were used for detection. The microwave frequency was stabilized to one part in 10^5 using an automatic frequency control (AFC) with a secondary lock-in at 8 kHz.

The photogeneration of ROS was evaluated under visible light illumination using EPR via the spin-trapping technique. The samples used in this study consisted of three suspensions in IPM with average compositions of 0.7(2) mmol L^{-1} Hyp and 5.6(3) mg/mL FF-NT, and all samples contained 200 mmol L^{-1} PBN. A Hyp sample with concentration of 9.9 mmol L^{-1} was also prepared using 200 mmol L^{-1} of PBN in IPM as a control. For the illumination, 218(2) μL of the IPM suspensions, which were already in the EPR quartz tubes, was exposed to light from a Xe-arc lamp (Oriel, 450 W, 15 V) after filtering out the infrared and short UV wavelengths using a water-filter and Pyrex windows, respectively. The sample tubes were illuminated inside a water thermal bath (room temperature) to ensure that the samples were not heated. The EPR signals were quantified using typical TEMPOL procedures.[33]

Computational Simulation Procedure. Computer simulations were performed to model the wall of the peptide nanotubes that were formed by the tubular subunits of the FF compounds in the presence of water. An investigation of the functionalization of hypericin at the nanotube surface was necessary. The initial atomic coordinates for the peptide nanotube were first described by Görbitz.[34,35] This crystal structure was used as a starting model for the molecular dynamics simulations performed herein. The computational cell was similar to that obtained in our previous work.[17] This cell consisted of three juxtaposed tube units with a length of 5.46 nm (10 dipeptide hexamers), which formed a surface area of 5.46 × 7.64 nm^2. (See the SI.) This system was placed in a water/hypericin box that was 8.40 nm tall. A similar box simulation, but without hypericin, was also prepared in an identical manner and used as the reference system. Atomistic molecular dynamic simulations were performed using GROMACS version 4.5,[36] and the Charmm27 force field[37] was employed to describe the interactions of the peptide nanotubes and the hypericin molecules. The interaction potential of the water molecule was described using the TIP3P model.[38] The system was investigated using the NPT ensemble under normal conditions (T = 300 K and p = 1 bar with periodic boundary conditions). As usual, the solute−solvent interactions were described using the Lennard-Jones and Coulomb potentials. Further details are provided in the SI.

RESULTS AND DISCUSSION

Morphology and X-ray Diffraction. Electron microscopy and fluorescence images from samples 1, 4, 7, and 10 (see Table 1) are shown in Figure 1. The fluorescence images, λ_{ex}/

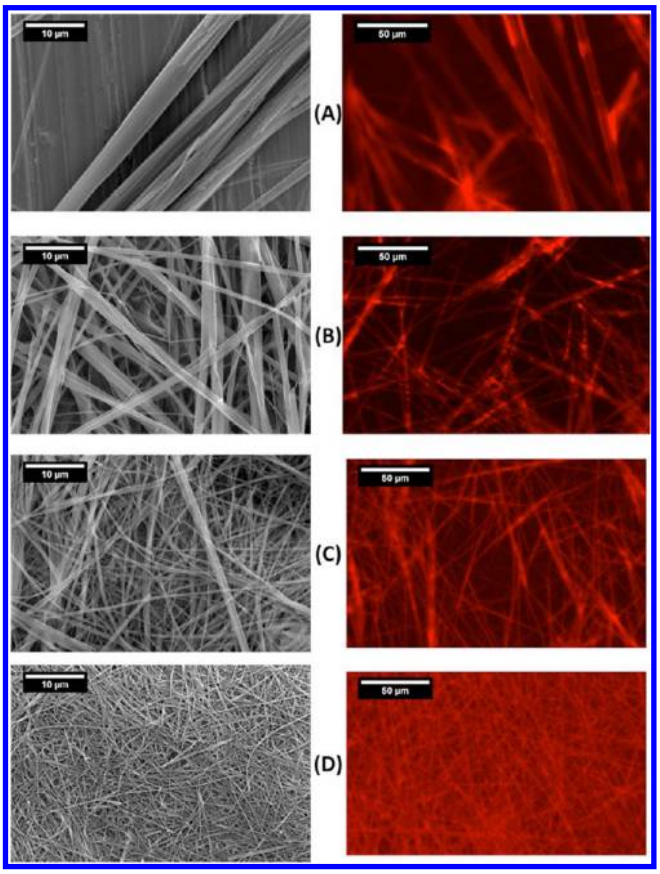

Figure 1. SEM and fluorescence images of the FF-NTs with Hyp concentrations at (A) 0.7, (B) 2.1, (C) 4.2, and (D) 6.0 μmol L^{-1}.

λ_{em} peaks at 535/590 nm, reveal that the distribution of hypericin onto the surface of the tubes is homogeneous, producing fluorescence emission throughout the structures. The tubular morphology of the assemblies is clearly revealed in electron microscopy micrographs with the appearance of the inner core (see SEM photographs in Figure 1A,B). A close dependence between the diameter of the tubes and the amount of Hyp is observed: higher concentrations of fluorophore lead to thinner structures. These findings can be explained by the disaggregation promoted by the interaction Hyp/peptide in agreement with previous studies, which have demonstrated that hypericin inhibits or interrupts the aggregation of peptides.[30,39]

The average diameter of the tubes, obtained from statistics over more than 100 counts in electron micrograph images, is exhibited as a function of the Hyp amount in Figure 2. The data are appropriately described by the following empirical law:

$$\text{Ø}_{\text{FFNT}} = 0.29 + 6.52 \times \exp(-0.83*[\text{Hyp}]) \quad (1)$$

where Ø_{FFNT} is the average diameter of the peptide assemblies and [Hyp] is the concentration of fluorophore. It should be noted that the choice of a first-order decay function to fit the experimental data in Figure 2 was arbitrary, and thus eq 1 cannot be interpreted as an universal behavior, applicable to fluorophore/FFNTs conjugates in general. Even so, it remains useful and provides interesting insights about the system

dx.doi.org/10.1021/jp3113655 | J. Phys. Chem. B XXXX, XXX, XXX−XXX

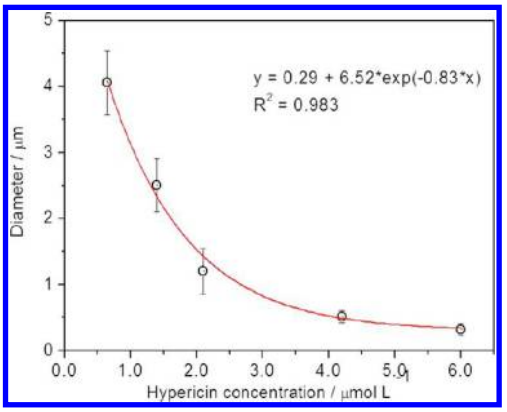

Figure 2. Correlation between the average diameters of the tube as a function of Hyp concentrations.

investigated here. By using this empirical relationship, we observe that $Ø_{FFNT}$ ranges from ~290 nm, at [Hyp] = 0, to ~7 μm at high concentrations. These values are in good agreement with the dimensions typically found for FF-based assemblies[3,4,6,11] in studies where physicochemical parameters, for example, concentration, temperature, solvent, and so on, are used in preparation to control the size of the structures. Here our findings point out that the concentration of Hyp is also a parameter able to drive the average diameter of the structures.

To obtain information regarding the conformational change of the nanotube that may be induced by the presence of Hyp, we recorded X-ray diffractograms. Unit cell parameters were obtained from Rietveld refinements (not shown) by using as inputs data previously obtained for the nanotube-only phase.[16] To this end, the general structure analysis system (GSAS)[40] software and its graphical user interface, EXPGUI,[41] were used. Neither the fractional coordinates nor the atomic displacement parameters were varied during the refinements. Figure 3 shows the XRD patterns of the FF-NT/Hyp with the same concentrations as the samples in Figure 1. The diffractograms found here are quite similar to those observed in the literature;[34,35] all of the Bragg reflections were appropriately indexed by a hexagonal space group $P6_1$ (Figure 3). In addition, a careful inspection of the profiles reveals the absence of extra reflections due to additional crystallographic phases. We observed that different Hyp concentrations alter the distance between the crystallographic planes, which results in different cell parameters. The major difference is observed in the cell parameter, *c*, which indicates that higher Hyp contents promote a larger distance between the crystallographic planes of the FF-NTs. The difference in cell parameters is illustrated in Figure 3. Although the lattice parameters *a* and *b* are very similar for assemblies prepared at distinct fluorophore concentrations, the value of *c* also increases as the Hyp concentration is increased. The interplay between the walls of the structures and fluorophore moieties occurs via interacting forces that describe the balance between Coulombic, π-stacking and van der Waals contributions. It is expected that fluorophore moieties can be found between the hexagonal planes indexed as belonging to the $P6_1$ space group. This result corroborates a previous work of our research group.[17]

Photophysical Characterization. In the excited state, the Hyp molecule transfers energy to oxygen with a high quantum yield, generating reactive species such as singlet oxygen (ROS). To determine the kinetics of ROS generation, we have used an indirect method employing the DPBF molecule as a suppressor, where type I and II mechanisms could be compromised. Both Hyp compounds and FF-NTs containing Hyp were dissolved in DMSO. A laser beam, wavelength at 590 nm, was coupled to the system for irradiation. Under continuous laser irradiation, UV/vis absorbance spectra were recorded every 20 s, and the decay of the DPBF absorbance at 417 nm (maximum absorption) was monitored as described elsewhere.[42,43] Thus plots of the absorbance versus time could be obtained in the time interval 0−600 s for the Hyp concentrations listed in Table 1. It should be noted that we have assumed that the absorbance is inversely proportional to the DPBF amount in DMSO. The determination of the decay rate of DBPF degradation as a function of the Hyp concentration (accordingly, the rate of ROS production upon the amount of fluorophore) is a key element in the current study because it allows us to quantify the changes on the photophysical properties of the hypericin after conjugation with peptide assemblies.

In Figure 4A, we show representative curves resulting from this procedure. A significant decaying of absorbance in time is clearly observed, an indication that the generation of ROS is effective either for FF-NTs-containing or FF-NTs-free solutions. Nevertheless, when Hyp appears conjugated with peptide assemblies, the decay rates of absorbance are considerably higher than those ones observed when only the

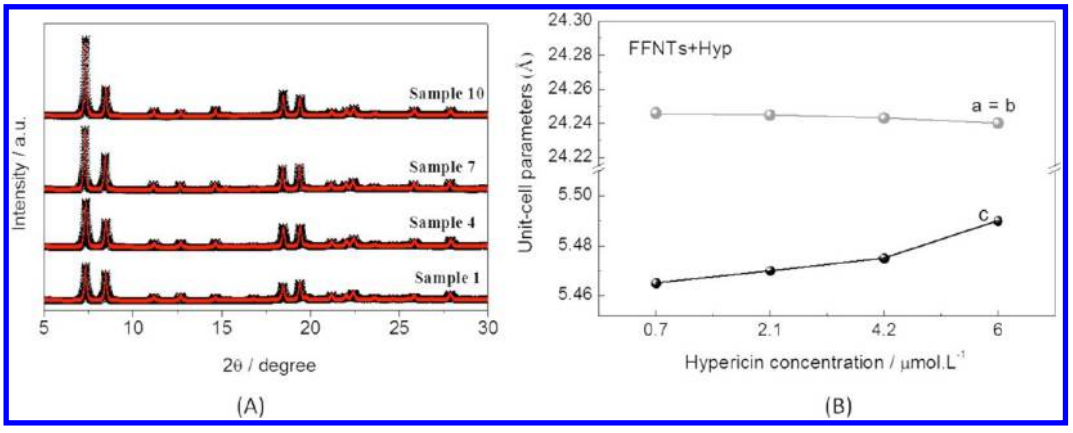

Figure 3. (A) Diffractograms from FF-NTs with different Hyp concentrations. (See Table 1.) The hexagonal space group *P*61 indexes perfectly the symmetry observed (ref 16). (B) Behavior of the lattice parameters showing the increase in parameter *c*, evidencing the intercalation of Hyp in the peptide matrix.

dx.doi.org/10.1021/jp3113655 | J. Phys. Chem. B XXXX, XXX, XXX−XXX

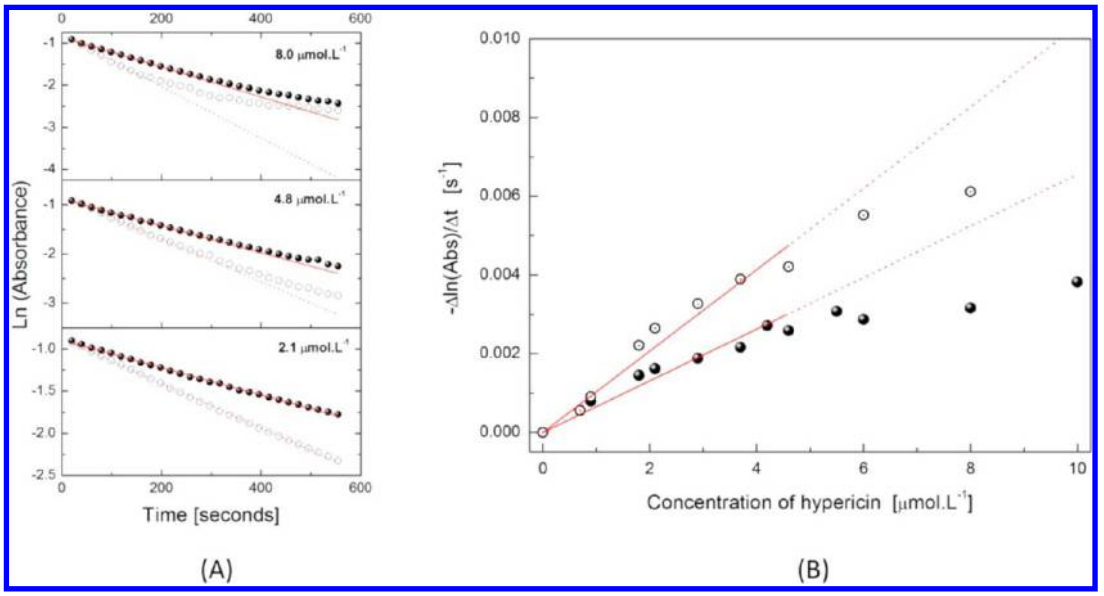

Figure 4. Open circles: FF-NTs-containg samples; filled spheres: bare hypericin samples. (A) Representative decay plots of the temporal absorbance of DPBF (at 417 nm). Red lines correspond to linear fits used to obtain the slope of the curves. (B) Degradation rate of DPBF as a function of hypericin concentration. Filled lines indicate the range used to perform fits from which kinetic constants of $k_{FF\text{-}NTs} = 1.03 \pm 0.05 \times 10^3$ L mol^{-1} s^{-1} and $k_{bare} = 6.55 \pm 0.28 \times 10^2$ L mol^{-1} s^{-1} were obtained for FF-NTs/Hyp and bare Hyp samples, respectively.

fluorophore is present. To quantitatively describe this behavior as a function of Hyp concentration, we have first determined slopes from first-order plots of absorbance in time, that is, from Ln(absorbance) versus time. The slopes were calculated from the linear part of the curves. This implies that for low Hyp amounts the values of $\Delta\ln(\text{Abs})/\Delta t$ could be obtained from fits performed over the entire time range (0−600 s, Figure 4A, bottom). As the concentration of fluorophore is increased, a deviation from the straight line appears due to DPBF consumption (Figure 4A, middle). For higher concentrations, the time range taken into account spanned between 0 and 160 s (Figure4A, top).

In the following, we used the values of $-\Delta\ln(\text{Abs})/\Delta t$ to calculate the rate of DPBF degradation as a function of the concentration of fluorophore (Figure 4B). We observe the production of ROS is clearly improved when FF-NTs are introduced in the system, as evidenced by a more rapid growth of the slopes under addition of Hyp. To quantify this behavior and bring an estimation on kinetic constants, the initial parts of the curves, [Hyp] < ∼5 μmol L^{-1}, were fitted to straight lines. The inclinations of these lines lead to kinetic constants of $k_{FF\text{-}NTs} = 1.03 \pm 0.05 \times 10^3$ L mol^{-1} s^{-1} and $k_{bare} = 6.55 \pm 0.28 \times 10^2$ L mol^{-1} s^{-1}, respectively, for FF-NTs/Hyp and bare Hyp samples. These findings show that the conjugation with peptide nanotubes leads to an improvement of ∼57% on the generation of ROS, probably due to the spatial organization of Hyp onto the surface of the assemblies and to assistance on charge transfers (see discussions below).

The fluorescence lifetimes were measured for samples 1, 4, 7, and 10 (the samples in Figure 1). Data from the fluorescence lifetimes were monitored at 590 nm with excitation at 540 nm. Table 2 shows the fluorescence lifetimes obtained from these samples. The fluorescence decays 44% more slowly for the FFNT/Hyp than for bare hypericin. Higher concentrations led to a slight decrease in the fluorescence lifetime because of the relative increase in the amount of hypericin in relation to the nanostructure. This result demonstrates that the presence of the L-diphenylalanine nanotube stabilizes the excited state of

Table 2. Fluorescence Lifetimes of Samples Produced Using Different FFNT/Hyp Concentrations

sample	$\tau \pm \sigma$ (ns)	χ^2
bare Hyp	2.719 ± 0.004	0.949
1	4.830 ± 0.006	1.367
4	4.833 ± 0.005	1.378
7	4.778 ± 0.005	1.353
10	4.733 ± 0.005	1.313

the photosensitizer due to the charge-transfer character. For longer fluorescence lifetimes, more energy is available to be transferred to the $^3O_2$, enhancing the ROS generation. This result is in agreement with the data obtained in the study of the indirect generation of singlet oxygen with DPBF, where the samples containing FF-NT/Hyp were more efficient than hypericin compounds.

Other factors may influence the increases in lifetime value, for example, the type of solvent, the concentration of hypericin and O_2, the adsorption process, or the presence of electron acceptors or donors.[44,45] Furthermore, considering that the NTs were synthesized in water, these increases in fluorescence lifetime could be attributed to the presence of residual water incorporated into the hydrophilic channel of the NTs. More recently, we have studied the electronic and energetic properties of FF-NTs using the self-consistent-charge density-functional-based tight binding method augmented with dispersion interactions (SCC-DFTB-D). These investigations point the presence of water molecules confined in the central hydrophilic channel of the assemblies. The interaction with water leads to the splitting of the conduction and valence bands and to a larger dispersion that perhaps could be associated with the alignment of the water molecules' dipole moments and eventually lead to a larger dipole moment of the overall structure. Thus, the presence of water molecules would increase the stability of hypericin in the excited state.

The photophysical properties of the modified peptide nanotubes were also investigated using EPR with spin trapping

dx.doi.org/10.1021/jp3113655 | J. Phys. Chem. B XXXX, XXX, XXX−XXX

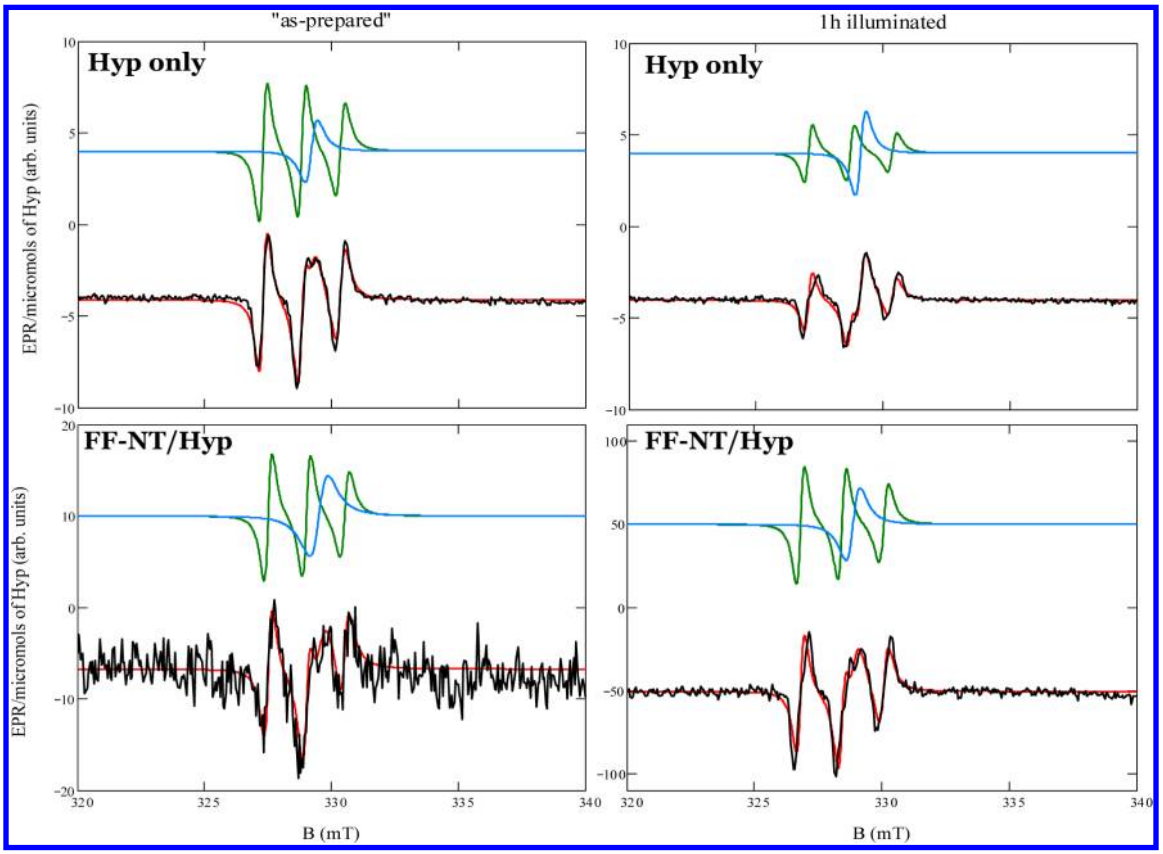

Figure 5. Room-temperature EPR spectra for the Hyp sample and the FF-NT/Hyp samples, both in IPM and using the PBN spin-trap. Left spectrum: "as-prepared" under ambient illumination. Right spectrum: after 1 h of illumination (Xe-arc lamp, 450 W). The experimental spectra are shown in black, whereas the best least-squares fits are shown in red. The green and blue spectra correspond to the PBN-OOH$^{\bullet}$ adduct and the radical Hyp^{-} lines, respectively. All spectra were normalized by the absolute number of moles of hypericin.

at room temperature, before and after illumination with visible light. The purpose of examining these properties was to obtain more details about the photogeneration of ROS with the FF-NT/Hyp and compare the results with pure hypericin samples. Isopropyl myristate (IPM), a common topic pharmaceutical vehicle used in sunscreens and insect repellents, was used as solvent, and PBN (200 mmol L^{-1}) was used as the spin-trap. After preparing the samples under ambient light, EPR measurements were performed before and after 1 h of illumination with a white-light high-power Xe arc lamp (450 W) in a water bath. Three FFNT/Hyp samples were studied, all of which had similar hypericin concentrations: 0.7(2) mmol L^{-1} Hyp and 5.6(3) mg/mL FF-NT. The fourth sample was a hypericin sample with 9.9(1) mmol L^{-1} Hyp.

Before illumination, all samples were measured as prepared under laboratory light. The preparation included weighing the reagents, dissolving, and sonicating. An average of 1 h under ambient fluorescent light was required for all samples. Under these conditions, all three samples presented EPR signals (normalized by Hyp concentration), as shown in Figure 5.

After 1 h of illumination with the Xe-arc lamp, all three samples containing FFNT/Hyp showed strongly amplified EPR signals. In contrast, the Hyp sample exhibited decreased EPR signals. All samples, including the Hyp, presented a similar EPR line pattern, which is composed of a triplet line spectrum due to the ^{14}N hyperfine structure of the PBN-OOH$^{\bullet}$ spin adduct (g = 2.0063 ± 0.0001 and $a_{hf}(^{14}N)$ = 15.9 ± 0.6 mT) that was formed by the reaction PBN + $O_2^{\bullet-}$ → PBN-OOH$^{\bullet}$ in the presence of water (in our case, residual) and a second single radical R$^{\bullet}$ line (g = 2.0031 ± 0.0001 and fwhm =1.0 ± 0.2 mT). The radical, R$^{\bullet}$, has the same g factor and a similar line width as the Hyp^{-} radical that appears in illuminated hypericin solutions.[26,27] This radical is also involved in the generation of superoxide by charge transfer (mechanism Type I), which is known to occur simultaneously with the formation of singlet oxygen (Type II mechanism) for illuminated Hyp solutions.[26,27] Therefore, we identified the R$^{\bullet}$ as Hyp^{-}.

The individual contributions to the overall spectra are also shown in Figure 5. The relative intensities of the EPR signals due to these two paramagnetic centers, PBN-OOH$^{\bullet}$ and Hyp^{-}, changed after the 1 h of light exposure and were the only free parameter in the line-shape analysis for all samples.

The quantification of the PBN-OOH$^{\bullet}$ adducts and Hyp^{-} species after double integration of the individual contributions to the total EPR spectra are shown in Table 3. As observed from Table 3, despite reduction of ∼55% in the PBN-OOH$^{\bullet}$ for the Hyp sample and lack of change in the Hyp^{-} concentration, all three FF-NT/Hyp samples showed a strong increase in PBN-OOH$^{\bullet}$ adducts and Hyp^{-} radicals per molecule of Hyp, with average factors of 9 ± 4 and of 3 ± 1, respectively. Furthermore, the spectra of the as-prepared samples revealed that despite the higher concentration of hypericin in the sample, the amount of PBN-OOH$^{\bullet}$ per molecule of hypericin is, accounting for the uncertainties, of the same order of magnitude for all samples.

On the basis of these results, we conclude that the illumination during sample preparation is sufficient to produce ROS in all suspensions. As mentioned previously, both Type I

dx.doi.org/10.1021/jp3113655 | J. Phys. Chem. B XXXX, XXX, XXX–XXX

Table 3. Concentration of the PBN-OOH$^{\bullet}$ and Hyp^{-} Radicals for All Samples Investigated Using the EPR Spin-Trapping Technique with PBN as a Spin-Trap[a]

sample	Hyp (mmol L^{-1})	conditions	PBN-OOH$^{\bullet}$ (per Hyp molecule)	Hyp^{-} species (per Hyp molecule)
Hyp	9.9(1)	as-prepared	1.1(2)	0.3(2)
		illuminated	0.5(2)	0.3(2)
A	0.5(1)	as-prepared	2.0(2)	1.9(2)
		illuminated	10.2(2)	5.6(2)
B	0.7(1)	as-prepared	0.4(2)	1.1(2)
		illuminated	6.3(2)	6.2(2)
C	0.9(1)	as-prepared	0.7(2)	1.6(2)
		illuminated	5.9(2)	4.4(2)

[a]"Illumination" as a condition indicates 1 h of illumination.

(electron transfer producing $O_2^{\bullet-}$) and Type II (energy transfer producing $^1O_2$) mechanisms are expected for the Hyp solution and thus also for the FFNT/Hyp suspensions. The detection of PBN-OOH$^{\bullet}$ in both types of samples indicates that the Type I mechanism is also occurring to some extent for the Hyp sample, as previously reported.[26] However, this mechanism is considerably more efficient for the FFNT/Hyp samples, even after 1 h of illumination, when a reduction of the PBN-OOH$^{\bullet}$ due to degradation is expected. In fact, the observed reduction of the PBN-OOH$^{\bullet}$ adducts in the hypericin solution after 1 h of illumination indicates that the degradation of PBN adducts occurs because of the considerable generation of singlet oxygen, which is not directly detectable using PBN spin-trapping. Evidence of the formation of superoxide, which is more efficient in the FFNT/Hyp suspensions than in the Hyp sample, is the increase in the Hyp^{-} radical under illumination for the former but not the latter. Hyp^{-} is an electron donor precursor of $O_2^{\bullet-}$ in the Type I mechanism. The increase in the PBN-OOH$^{\bullet}$ adducts in the FF-NT/Hyp after 1 h of illumination is approximately three times that of Hyp^{-}. This result may indicate that the degradation of PBN adducts due to the presence of singlet oxygen is hindered or that another electron donor is involved in the formation of the superoxide. The latter contribution to this mechanism is greater than that of Hyp^{-}. Therefore, we propose that the enhanced production of superoxide in the case of FF-NT/Hyp occurs due to electron transfer from the NT to oxygen molecules and therefore that the Type I mechanism is dominant for the FFNT/Hyp samples.

Computational Results. Our simulations allow us to analyze the structural properties of the hypericin solution on the nanotube surface. In this sense, an interesting aspect to be observed is the possible functionalization of the nanotube by these amphiphilic species. We analyzed the structural and dynamical properties of the nanotube aqueous solutions after 20 ns simulations. Because hypericins are polyaromatic, they have significant π-stacking interactions. This interaction is responsible for the aggregation pattern observed in the aqueous environment, in which the hypericin molecules precipitate in long chains and are deposited on the surface of the tube, as shown in Figure 6.

Figure 7 presents the mass density profiles (along the z direction) for the system components and an atomistic representation of the system. Note that the water profile does not present a pronounced peak near the nanotube surface. Instead, the density smoothly increases from the surface, which indicates that the water molecules interact with the polar sites of the hypericin molecules and can permeate these molecules to be closer to the nanotube. Inside the tube, we can see a larger structuration of water molecules, which interact with the inner wall and present a clear confinement pattern with a hydration shell near the internal surface and a peak concentration on the tube axis.

We can visualize the local adsorption structure using the spatial distribution function of the hypericin molecules near the nanotube surface. (See Figure 7.) The hypericin molecules tend to isotropically adsorb at the surface of the nanotube, and their spatial distribution is highly localized, which suggests that the molecule remains bound in the position where it was adsorbed, forming a thin coating layer. AFM imaging performed on FFNT/Hyp corroborates the adsorption of the fluorophore onto the surface of the tubes (see SI, Figure S4).

Evidence of this functionalization can be obtained by comparing the distribution of water molecules in both systems, with and without hypericin molecules. In Figure 8, the difference between the two profiles indicates the volume of

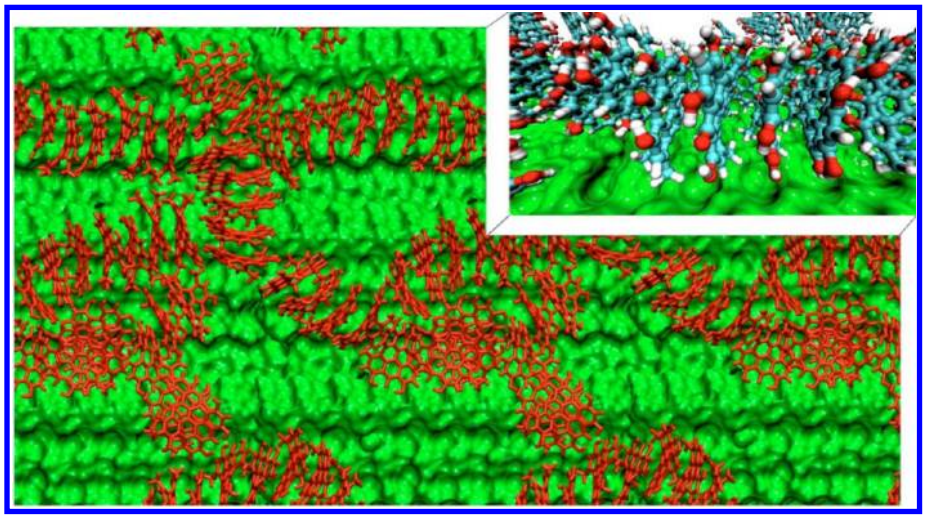

Figure 6. Perpendicular view (XY plane) showing the pattern of adsorbed stacked hypericin molecules on the nanotube surface. Highlighted, we present a magnified view of the nanotube surface (in green) and the interactions among the molecules of hypericin and the peptide nanotube.

dx.doi.org/10.1021/jp3113655 | J. Phys. Chem. B XXXX, XXX, XXX–XXX

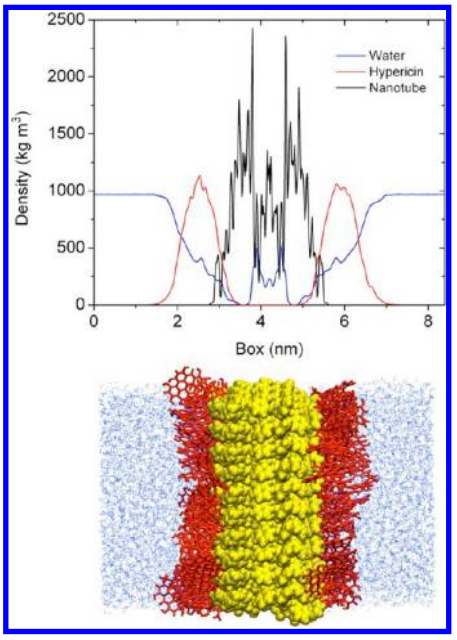

Figure 7. Mass density distribution (kg m^{-3}) computed for the components of the molecular system and a representative view of a molecular configuration. The density of the fluid phase from the nanotube surface varies considerably along the z direction. Water, hypericin molecules, and the peptide nanotube are shown in blue, red, and yellow, respectively.

water molecules displaced from the surface of the tube due to the adsorption of hypericin. The neutral system exhibits a clear peak in the water density profile near the surface of the nanotube, which results from the hydrophobic repulsion from the tube wall. This peak does not exist for ionic systems, and the water molecules in the hypericin-containing system can interact strongly with the carboxylic groups.

The change in the electrostatic behavior of the surface can also be analyzed in terms of the mobility of the water molecules near the surface of the tube for the two situations analyzed here: with and without hypericin. To examine the translational motion of the molecules along the nanotube surface, we have computed the lateral MSD by averaging over the center-of-mass of the water molecules in the *XY* plane. (See Figure 9.) Here we have considered the motion of the liquid water to be parallel to the nanotube surface for both solutions. Although the motion at long times maintains the linear diffusive regime for both systems, there are appreciable differences in the lateral diffusion coefficients. Our calculated lateral diffusion coefficients for the systems with and without hypericin are 4.33 ± 0.04 and 5.54 ± 0.11 nm^2 ns^{-1}, respectively, and we observed that the diffusion is faster for the isolated system than for its counterpart containing hypericin. This result can be understood through the electrostatic interactions between the adsorbed hypericin and water. These changes also indicate a possible functionalization effect through the nanotube surface.

CONCLUSIONS

In this study, L-diphenylalanine micro/nanotubes (FF-NTs) were functionalized with Hyp, and their structural and photophysical properties were examined. Using the liquid-phase approach, the tubes were self-assembled and functionalized with Hyp at concentrations ranging from 0.7 to 10 μmol L^{-1}. For higher Hyp concentration, the formed structures are thinner in the comparison with those ones obtained at lower amounts of chromophore, demonstrating that hypericin inhibits or interrupts the aggregation of peptides. XRD patterns indicate that the symmetry of the molecular arrangement is appropriately indexed by the crystallographic space group $P6_1$. Interestingly, an increase in the c lattice parameter is observed upon the addition of Hyp, which is interpreted as evidence that fluorophore appears embedded in the assemblies. To assess the interaction of the Hyp with the FF-NTs, we conducted molecular dynamics simulations. These studies revealed the intercalation of the fluorophore into the peptidic matrix. This result indicated the presence of a uniform surface coating and reduced lateral diffusion of water in the system containing Hyp, which is supported by the fluorescence and SEM images. The generation of ROS by the functionalized material was studied using UV/vis spectroscopy and EPR spin-trapping techniques. Both measurements indicate that the production of ROS is faster and more efficient for the FF-NTs/Hyp system. This result is explained by either Type I or Type II mechanisms, which are enhanced in the case of the FF-NTs/Hyp hybrid structure due to electron transfer from the NTs to oxygen molecules with the formation of superoxide species (Type I mechanism). Lifetime measurements reveal that the introduction of peptidic structures also increases the endurance of the reactive species (4.8 ns for FF-NT/Hyp and 2.7 ns for bare Hyp). The improvement on photophysical properties of hypericin has been attributed to its spatial organization onto the surface of peptide assemblies, which could assist or induce charge-transfer processes.

Despite the fact that both in vitro and in vivo toxicity experiments are still necessary to evaluate the utilization of these complexes under more realistic conditions for applica-

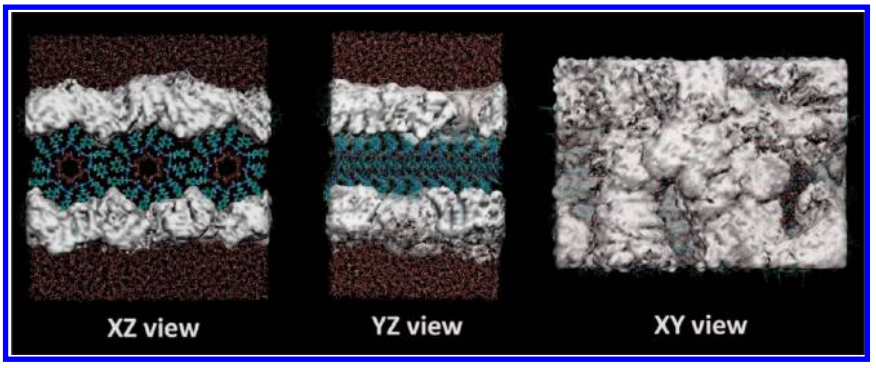

Figure 8. Hypericin spatial distribution function (in gray). The surface has been drawn in a local nanotube frame.

dx.doi.org/10.1021/jp3113655 | J. Phys. Chem. B XXXX, XXX, XXX–XXX

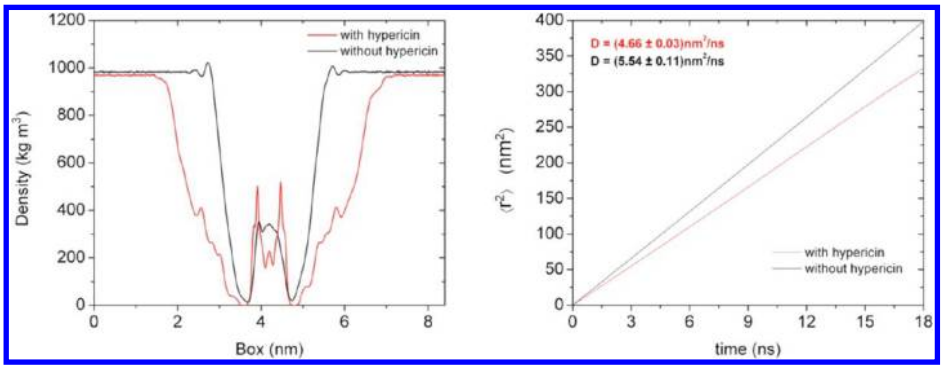

Figure 9. Comparison between the water mass density distributions (kg m^{-3}) computed for the systems with and without hypericin molecules. Lateral diffusion coefficients (in nm^2 ns^{-1}) for the water molecules calculated using a linear fit of the MSD from 2 to 18 ns.

tions in photodynamical therapy, our results clearly demonstrate the potential of peptide assemblies to enhance the generation of ROS by light-sensitive compounds.

■ ASSOCIATED CONTENT

Supporting Information

Computational and AFM imaging details. This material is available free of charge via the Internet at http://pubs.acs.org.

■ AUTHOR INFORMATION

Corresponding Author

*E-mail: wendel.alves@ufabc.edu.br. Tel: +55 11 4996 0193. Fax: +55 11 4996 3166.

Notes

The authors declare no competing financial interest.

■ ACKNOWLEDGMENTS

Financial support by the Brazilian agencies *Fundação de Amparo à Pesquisa do Estado de São Paulo* (FAPESP, grant no. 08/53576-9) and *Fundação de Amparo à Pesquisa do Estado de Minas Gerais* (FAPEMIG, grant no. APQ 02000-10) is gratefully acknowledged. This work was also supported by INCT in Bioanalytics (FAPESP, grant no. 08/57805-2 and CNPq, grants no. 573672/2008-3) and CNPq (grant no. 472197/2012-6). We are thankful to LME-LNLS for the use of SEM facilities, and we also thank Professor Teresa Atvars from University of Campinas and Dr. Tatiana Duque Martins from Federal University of Goias for the fluorescence spectroscopy measurements. We are also grateful to Luciano Gabriel Silva for helping us with sample preparation and obtaining the EPR spectra. The MTA staff (Raul Freitas, Vinícius Pimentel, Evandro Lanzoni and Christoph Deneke) at LNNano is kindly acknowledged for helpful discussions and assistance during AFM experiments (proposal AFM-NSIIIa - 14611). E.R.S.thanks PNPD-CAPES for a postdoctoral fellowship.

■ REFERENCES

(1) Si, W.; Hu, X.-B.; Liu, X.-H.; Fan, R.; Chen, Z.; Weng, L.; Hou, J.-L. Self-Assembly and Proton Conductance of Organic Nanotubes from Pillar[5]arenes. *Tetrahedron Lett.* **2011**, *52*, 2484−2487.

(2) Toksöz, S.; Guler, M. O. Self-Assembled Peptidic Nanostructures. *Nano Today* **2009**, *4*, 458−469.

(3) Demirel, G.; Buyukserin, F. Surface-Induced Self-Assembly of Dipeptides onto Nanotextured Surfaces. *Langmuir* **2011**, *27*, 12533−12538.

(4) Reches, M.; Gazit, E. Casting Metal Nanowires Within Discrete Self-Assembled Peptide Nanotubes. *Science* **2003**, *300*, 625−627.

(5) Tamamis, P.; Adler-Abramovich, L.; Reches, M.; Marshall, K.; Sikorski, P.; Serpell, L.; Gazit, E.; Archontis, G. Self-Assembly of Phenylalanine Oligopeptides: Insights from Experiments and Simulations. *Biophys. J.* **2009**, *96*, 5020−5029.

(6) Yemini, M.; Reches, M.; Rishpon, J.; Gazit, E. Novel Electrochemical Biosensing Platform Using Self-Assembled Peptide Nanotubes. *Nano Lett.* **2004**, *5*, 183−186.

(7) Yan, X.; Su, Y.; Li, J.; Früh, J.; Möhwald, H. Uniaxially Oriented Peptide Crystals for Active Optical Waveguiding. *Angew. Chem., Int. Ed.* **2011**, *50*, 11186−11191.

(8) Yan, X.; Zhu, P.; Fei, J.; Li, J. Self-Assembly of Peptide-Inorganic Hybrid Spheres for Adaptive Encapsulation of Guests. *Adv. Mater.* **2010**, *22*, 1283−1287.

(9) Yan, X.; Cui, Y.; Qi, W.; Su, Y.; Yang, Y.; He, Q.; Li, J. Self-Assembly of Peptide-Based Colloids Containing Lipophilic Nanocrystals. *Small* **2008**, *4*, 1687−1693.

(10) Yan, X.; Zhu, P.; Li, J. Self-Assembly and Application of Diphenylalanine-Based Nanostructures. *Chem. Soc. Rev.* **2010**, *39*, 1877−1890.

(11) de la Rica, R.; Matsui, H. Applications of Peptide and Protein-Based Materials in Bionanotechnology. *Chem. Soc. Rev.* **2010**, *39*, 3499−3509.

(12) Matos, I. O.; Alves, W. A. Electrochemical Determination of Dopamine Based on Self-Assembled Peptide Nanostructure. *ACS Appl. Mater. Interfaces* **2011**, *3*, 4437−4443.

(13) de la Rica, R.; Mendoza, E.; Matsui, H. Bioinspired Target-Specific Crystallization on Peptide Nanotubes for Ultrasensitive Pb Ion Detection. *Small* **2010**, *6*, 1753−1756.

(14) Ryu, J.; Park, C. B. Synthesis of Diphenylalanine/Polyaniline Core/Shell Conducting Nanowires by Peptide Self-Assembly. *Angew. Chem., Int. Ed.* **2009**, *48*, 4820−4823.

(15) Kim, J. H.; Lim, S. Y.; Nam, D. H.; Ryu, J.; Ku, S. H.; Park, C. B. Self-Assembled, Photoluminescent Peptide Hydrogel as a Versatile Platform for Enzyme-Based Optical Biosensors. *Biosens. Bioelectron.* **2011**, *26*, 1860−1865.

(16) Cipriano, T.; Takahashi, P.; de Lima, D.; Oliveira, V.; Souza, J.; Martinho, H.; Alves, W. A. Spatial Organization of Peptide Nanotubes for Electrochemical Devices. *J. Mater. Sci.* **2010**, *45*, 5101−5108.

(17) Martins, T. D.; Souza, M. I.; Cunha, B. B.; Takahashi, P. M.; Ferreira, F. F.; Souza, J. A.; Fileti, E. E.; Alves, W. A. Influence of pH and Pyrenyl on the Structural and Morphological Control of Peptide Nanotubes. *J. Phys. Chem. C* **2011**, *115*, 7906−7913.

(18) Karioti, A.; Bilia, A. R. Hypericins as Potential Leads for New Therapeutics. *Int. J. Mol. Sci.* **2010**, *11*, 562−594.

(19) Gbur, P.; Dedic, R.; Chorvat, D., Jr.; Miskovsky, P.; Hala, J.; Jancura, D. Time-Resolved Luminescence and Singlet Oxygen Formation After Illumination of the Hypericin-Low-Density Lipoprotein Complex. *Photochem. Photobiol.* **2009**, *85*, 816−823.

(20) Sánchez-Cortés, S.; Miskovsky, P.; Jancura, D.; Bertoluzza, A. Specific Interactions of Antiretroviraly Active Drug Hypericin with DNA as Studied by Surface-Enhanced Resonance Raman Spectroscopy. *J. Phys. Chem.* **1996**, *100*, 1938−1944.

(21) Guedes, R. C.; Eriksson, L. A. Theoretical Study of Hypericin. *J. Photochem. Photobiol., A* **2005**, *172*, 293−299.
(22) Arabei, S. M.; Galaup, J. P.; Jardon, P. Analysis of the Site Selected Fluorescence and the Phosphorescence Spectrum of Hypericin in Ethanol. *Chem. Phys. Lett.* **1997**, *270*, 31−36.
(23) Weiner, L.; Mazur, Y. EPR Studies of Hypericin. Photogeneration of Free Radicals and Superoxide. *J. Chem. Soc., Perkin Trans.* **1992**, *2*, 1439−1442.
(24) Sgarbossa, A.; Lenci, F. Spectroscopic Study of Visible-Light Effects on Hypericin-Lens Proteins Systems. *Photochem. Photobiol.* **2001**, *74*, 196−200.
(25) Hamblin, M. R.; Hasan, T. Photodynamic Therapy: A New Antimicrobial Approach to Infectious Disease? *Photochem. Photobiol. Sci.* **2004**, *3*, 436−450.
(26) Asilian, A.; Davami, M. Comparison Between the Efficacy of Photodynamic Therapy and Topical Paromomycin in the Treatment of Old World Cutaneous Leishmaniasis: A Placebo-Controlled, Randomized Clinical Trial. *Clin. Exp. Dermatol.* **2006**, *31*, 634−637.
(27) Enk, C. D.; Fritsch, C.; Jonas, F.; Nasereddin, A.; Ingber, A.; Jaffe, C. L.; Ruzicka, T. Treatment of Cutaneous Leishmaniasis with Photodynamic Therapy. *Arch. Dermatol.* **2003**, *139*, 432−434.
(28) Gardlo, K.; Horska, Z.; Enk, C. D.; Rauch, L.; Megahed, M.; Ruzicka, T.; Fritsch, C. Treatment of Cutaneous Leishmaniasis by Photodynamic Therapy. *J. Am. Acad. Dermatol.* **2003**, *48*, 893−896.
(29) Gardlo, K.; Hanneken, S.; Ruzicka, T.; Neumann, N. J. Photodynamic Therapy of Cutaneous Leishmaniasis. A Promising New Therapeutic Modality. *Hautarzt* **2004**, *55*, 381−383.
(30) Bramanti, E.; Lenci, F.; Sgarbossa, A. Effects of Hypericin on the Structure and Aggregation Properties of β-Amyloid Peptides. *Eur. Biophys. J.* **2010**, *39*, 1493−1501.
(31) Falk, H.; Meyer, J.; Oberreiter, M. A Convenient Semisynthetic Route to Hypericin. *Monatsh. Chem.* **1993**, *124*, 339−341.
(32) Huygens, A.; Kamuhabwa, A. R.; de Witte, P. A. Stability of Different Formulations and Ion Pairs of Hypericin. *Eur. J. Pharm. Biopharm.* **2005**, *59*, 461−468.
(33) Wilcox, C. S. Effects of Tempol and Redox-Cycling Nitroxides in Models of Oxidative Stress. *Pharmacol. Ther.* **2010**, *126*, 119−145.
(34) Görbitz, C. H. Nanotube Formation by Hydrophobic Dipeptides. *Chem.—Eur. J.* **2001**, *7*, 5153−5159.
(35) Görbitz, C. H. The Structure of Nanotubes Formed by Diphenylalanine, the Core Recognition Motif of Alzheimer's β-Amyloid Polypeptide. *Chem. Commun.* **2006**, 2332−2334.
(36) Hess, B.; Kutzner, C.; van der Spoel, D.; Lindahl, E. GROMACS 4: Algorithms for Highly Efficient, Load-Balanced, and Scalable Molecular Simulation. *J. Chem. Theory Comput.* **2008**, *4*, 435−447.
(37) MacKerell, A. D.; Bashford, D.; Bellott, M.; Dunbrack, R. L.; Evanseck, J. D.; Field, M. J.; Fischer, S.; Gao, J.; Guo, H.; Ha, S.; et al. All-Atom Empirical Potential for Molecular Modeling and Dynamics Studies of Proteins. *J. Phys. Chem. B* **1998**, *102*, 3586−3616.
(38) Jorgensen, W. L.; Chandrasekhar, J.; Madura, J. D.; Impey, R. W.; Klein, M. L. Comparison of Simple Potential Functions for Simulating Liquid Water. *J. Chem. Phys.* **1983**, *79*, 926−935.
(39) Sgarbossa, A.; Buselli, D.; Lenci, F. In Vitro Perturbation of Aggregation Processes in β-Amyloid Peptides: A Spectroscopic Study. *FEBS Lett.* **2008**, *582*, 3288−3292.
(40) Larson, A. C.; Von Dreele, R. B. *General Structure Analysis System (GSAS) (Report LAUR 86−748)*; Los Alamos National Laboratory: Los Alamos, NM, 2001.
(41) Toby, B. H.; EXPGUI, A. Graphical User Interface for GSAS. *J. Appl. Crystallogr.* **2001**, *34*, 210−213.
(42) Spiller, W.; Kliesch, H.; Wohrle, D.; Hackbarth, S.; Roder, B.; Schnurpfeil, G. Singlet Oxygen Quantum Yields of Different Photosensitizers in Polar Solvents and Micellar Solutions. *J. Porphyrins Phthalocyanines* **1998**, *2*, 145−158.
(43) Engelmann, F. M.; Mayer, I.; Araki, K.; Toma, H. E.; Baptista, M. S.; Maeda, H.; Osuka, A.; Furuta, H. Photochemistry of Doubly *N*-Confused Porphyrin Bonded to Non-Conventional High Oxidation State Ag(III) and Cu(III) Ions. *J. Photochem. Photobiol., A* **2004**, *163*, 403−411.
(44) Redmond, R. W.; Land, E. J.; Truscott, T. G. Aggregation Effects on the Photophysical Properties of Porphyrins in Relation to Mechanisms Involved in Photodynamic Therapy. *Adv. Exp. Med. Biol.* **1985**, *193*, 293−302.
(45) Falk, H.; Meyer, J. On the Homo- and Heteroassociation of Hypericin. *Monatsh. Chem.* **1994**, *125*, 753−762.